

**YBCO Step Edge Josephson Junction:  
Fabrication, Characterization, Modeling  
and Applications**

**SANDEEP KUMAR**



**DEPARTMENT OF PHYSICS  
INDIAN INSTITUTE OF TECHNOLOGY DELHI**

**July 2025**

**© Indian Institute of Technology Delhi (IITD), New Delhi, 2025**

**YBCO Step Edge Josephson Junction: Fabrication,  
Characterization, Modeling and Applications**

**by**

**SANDEEP KUMAR**

**Department of Physics**

**Submitted**

**in fulfilment of the requirements for the degree of Doctor  
of Philosophy to the**



**DEPARTMENT OF PHYSICS  
INDIAN INSTITUTE OF TECHNOLOGY DELHI**

**July 2025**

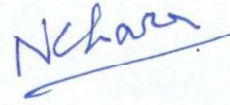
*Dedicated  
to  
my family*

## CERTIFICATE

---

This is to certify that the thesis entitled “**YBCO Step Edge Josephson Junction: Fabrication, Characterization, Modeling And Applications**” being submitted by Sandeep Kumar to the Department of Physics, Indian Institute of Technology Delhi is worthy of consideration for the award of the degree of Doctor of Philosophy and is a record of the original Bonafide research work carried out by him under my guidance and supervision. He has fulfilled all the criteria for the submission of the thesis, which in my opinion has reached the necessary standard.

The results contained in this thesis have not been submitted, in part or full, to any other university or institute for the award of any degree or diploma.



Prof. Neeraj Khare  
Department of Physics  
Indian Institute of Technology Delhi  
Hauz Khas, New Delhi-110016, India

## ACKNOWLEDGMENTS

---

---

*I am grateful to the Almighty God for his endless blessings, guidance, and strength, which have been a constant source of inspiration throughout my journey. His grace has instilled in me resilience and positivity. I extend my sincere appreciation to my supervisor, Prof. Neeraj Khare, for his invaluable guidance, encouragement, and expertise. His unwavering support and insightful mentorship have been instrumental in shaping this research. The knowledge and wisdom I have gained under his guidance will have a lasting impact on my academic and professional growth.*

*I am deeply grateful to my Student Research Committee (SRC) members, Prof. Sujeet Chaudhary, Prof. Pankaj Srivastava, and Prof. Samaresh Das, for their continuous evaluation of my research progress at every stage and for providing invaluable suggestions that have greatly contributed to its improvement. Furthermore, I would like to express my gratitude to the DRC chairperson of the Physics Department at IIT Delhi for generously dedicating his time and offering support in overseeing the progress of my research work. I also wish to thank the Nanoscale Research Facility (NRF), Central Research Facility (CRF), and the Physics Department at IIT Delhi for providing access to various fabrication, characterization, and measurement facilities and all the technical staff of IIT Delhi for their assistance in completing my research work.*

*I also wish to express my sincere gratitude to Dr. Sangeeta Khare for her generous support and willingness to share her knowledge and experiences. Her valuable insights have broadened my perspective and significantly contributed to the progress of this research.*

*I extend my heartfelt gratitude to my colleagues at the Nano Functional Oxides and Superconductivity Laboratory (NFOSL), including Dr. Mohd. Faraz, Dr. Deepanshu Sharma, Dr. Rohit Kumar, Dr. Huidrom Hemojit Singh, Dr. Dheeraj Kumar, Dr. Mamta Dahiya, Dr. Amish Kumar Gautam, Dr. Mohit Khosya, Dr. Birendra Kumar, Dr. Gaurav Sharma, Mrs.*

*Abhilasha Chouksey, Mr. Aman Sharma, Mr. Gaurav Kumar, Dr. Manoj Singh, Dr. Arum Mondal, Ms. Rajni, and Ms. Sarita. Their support and contributions have been invaluable in creating a conducive working environment in the lab. I offer special thanks to Dr. Mamta Dahiya for generously sharing her experiences, knowledge, constant motivation, and all the discussions, which have been particularly beneficial to me. From each labmate, I have gained valuable insights and knowledge. I extend my best wishes to all of them for success in their future endeavours. I sincerely thank the M.Tech (Ms. Shraddha Singhal) and B.Tech students (Mr. Neelkanth, Mr. Ayan, and Ms. Amrita) with whom I collaborated on project works for their invaluable support and engaging discussions.*

*I deeply appreciate the unwavering support and blessings of my grandparents, Mrs. Sita Devi and Mr. Ved Prakash Goyal; my parents, Mrs. Kamlesh Goyal and Mr. Pawan Goyal; My brother, Mr. Rahul Goyal. A special thanks to Mrs. Akshi Gupta for her constant support throughout the Journey of my life. I would like to extend my thanks to my aunt, Mrs. Rani Kansal; my cousins, Ms. Jyoti Kansal and Mr. Vishal Kansal. I would like to thank Mrs. Sonia Gupta and Mr. Ravinder Gupta for their forever love, blessings and support. I would also like to thank Mrs. Suniksha Gupta, her husband Mr. Antriksh Agarwal for their support. I owe my success to their constant backing, and I dedicate this thesis to my family as a token of gratitude. I would also like to express my gratitude to my mentors, Prof. Sushil Kumar and Prof. Dharamvir Singh Ahlawat, for their support and encouragement in guiding me toward the field of research.*

*I sincerely thank my dear friends, Mr. Siddharth Rana, Mr. Harvinder Ahuja, Ms. Sarita Mittal, Ms. Sneha Senapati, Mr. Jaswant Singh and his wife Mrs. Anita, Mr. Kamlesh Bhatt, Mr. Uzair Alam, and Mr. Harish Khan for their unwavering support, companionship, and the countless cherished memories we have shared throughout my PhD journey. Their presence has made this experience truly special and unforgettable. I am also thankful for the opportunities, challenges,*

*and experiences that have contributed to my learning and growth. The journey of research has been both enriching and fulfilling, and I cherish the knowledge and skills I have acquired along the way.*

*Finally, I sincerely acknowledge the Ministry of Electronics and Information Technology (MeitY) and the Department of Science and Technology (DST), India, for their generous financial support for this research. I am also deeply grateful to the University Grants Commission (UGC) for awarding me the Junior Research Fellowship (JRF) and Senior Research Fellowship (SRF), which greatly supported me throughout my PhD journey.*



**Sandeep Kumar**

## ABSTRACT

---

---

High temperature superconductors-based Josephson junctions have brought a new revolution in the field of superconducting electronics as they can be operated at temperatures that are achievable with single-stage cryocoolers or liquid nitrogen, which is very economical as compared to liquid helium or helium-based multistage cryocoolers.  $\text{YBa}_2\text{Cu}_3\text{O}_{7-x}$  (YBCO) is the most suitable high temperature superconductor because of its high critical temperature (92 K) and ease of preparation. There are various ways through which Josephson junctions based on high temperature superconductors are fabricated; among them, step edge junctions are preferred because of their ease of fabrication and flexibility of placing them anywhere on the substrate, which makes it feasible to make high density array of Josephson junctions. However, the  $I_c R_n$  product (also called the characteristic voltage) of the step edge junctions is low, and techniques are required to improve their  $I_c R_n$  product.

In the present work, the step edge Josephson junctions are fabricated on MgO (100) substrates using the standard photolithography and ion beam etching techniques, while the superconducting film is deposited using the pulsed laser deposition (PLD) technique. In order to tune the properties of step edge Josephson junctions, the effect of step angle and the width of the microbridge is studied. The step angle is varied by varying the direction of the ion beam falling relative to the substrate, which is done by placing the substrate at different orientations with respect to the ion beam. The step angle is varied from  $10^\circ$  to  $35^\circ$  and the microbridge width and length are kept as  $10\ \mu\text{m}$  and  $100\ \mu\text{m}$  respectively. It is found that as the step angle increases, the critical current ( $I_c$ ) of the junction drops while its normal state resistance ( $R_n$ ) rises. The overall  $I_c R_n$  product is found to be increasing with an increase in the step angle at all temperatures from 68 K to 77 K. For the  $35^\circ$  step angle junction, the  $I_c R_n$  value is obtained to be 0.34 mV at 77 K. For lower step angle junctions, the superconductor grain to grain coupling exhibits more superconductor-normal-superconductor (SNS) type behavior, but as the step

angle increases, the superconductor-insulator-superconductor (SIS) type behavior becomes apparent. For studying the effect of microbridge width on the transport properties, the microbridge width is varied from 20  $\mu\text{m}$  to 2  $\mu\text{m}$  while keeping the step angle fixed as  $\sim 19^\circ$  and the microbridge length as 100  $\mu\text{m}$ . A decrease in the critical current ( $I_c$ ) and an increase in the normal state resistance ( $R_n$ ) of the step edge junctions are observed with a decrease in the width of the microbridge, while the  $I_c R_n$  product increases with a reduction in the microbridge width. The critical current density value is found to be maximum for the 2  $\mu\text{m}$  wide junction. The behavior of all the junctions is superconductor-normal metal-superconductor (SNS) type. The  $I_c R_n$  product for the junction with a 2  $\mu\text{m}$  wide microbridge is obtained as 0.4 mV at 77 K. When the step angle is taken to be  $\sim 35^\circ$  and the microbridge width to be 2  $\mu\text{m}$  the  $I_c R_n$  product of the step edge Josephson junction is found to be  $\sim 0.52$  mV.

In order to understand the exact nature of the step edge Josephson junction, the I-V characteristics of the step edge Josephson junctions are simulated using the resistively capacitively shunted junction (RCSJ) model and compared with experimental results of step edge junction with step angle of  $\sim 35^\circ$ , and microbridge width of 2  $\mu\text{m}$ . When the I-V curves are simulated using the RCSJ model considering a single junction forming at the step edge, the simulated data does not fit with experimental data. However, when the I-V curves are simulated using the RCSJ model considering two Josephson junctions connected in series, the simulated data fits well with the experimental data. Comparison of the simulated curves with the experimental curves at different temperatures indicates that the noise factor increases with increasing temperature.

Another possible method to enhance the  $I_c R_n$  product of the junction is to induce oxygen vacancies in the junction area, which is achieved here by irradiating the junction area with Argon (Ar) ions for various time intervals varying from 1 min to 6 min. The junction has a step angle of  $\sim 35^\circ$ , and a microbridge width of 2  $\mu\text{m}$ . It is found that with the increase in the

exposure time of Ar ion irradiation, the value of  $I_c$  decreases, and the  $R_n$  value increases. The value of  $I_c \sim 70 \mu\text{A}$  and  $R_n$  value of  $\sim 9.4 \Omega$  have been observed at 77 K after irradiating for 4 min so that the  $I_c R_n$  product of the junction is achieved to be  $\sim 0.66 \text{ mV}$  at 77 K.

Finally, a DC Superconducting Quantum Interference Device (SQUID) is fabricated on STO (100) substrate using step edge Josephson junctions. SQUID has two parallel step edge Josephson junctions with a microbridge width of  $2 \mu\text{m}$  and length of  $50 \mu\text{m}$  and a loop area of  $20 \times 50 \mu\text{m}^2$ . The electrical transport properties, such as R-T and I-V, and voltage-flux characteristics are studied. Furthermore, it is observed that with the increasing number of thermal cycles, the critical temperature of the device decreases, and the wettability of the device increases. In order to increase the stability of the device, passivation of the device is done using the S1813 photoresist layer. It is found that the passivated device becomes water repellent, its contact angle is  $108^\circ$  and does not deteriorate with long time exposure to moisture. The transport properties of the passivated device are found to remain unaffected as compared to the bare device, which makes the passivation technique effective for the operation of YBCO based devices using liquid nitrogen cryostats. The voltage-flux characteristics of the passivated SQUID are observed for a magnetic field of amplitude  $6 \times 10^{-7} \text{ T}$ . The period of one modulation corresponds to a magnetic field of  $1.2 \times 10^{-7} \text{ T}$ . The sensitivity of the SQUID is  $\sim 10^{-10} \text{ THz}^{-1/2}$ .

## सार

उच्च तापमान अतिचालकों पर आधारित जोसेफसन जंक्शन ने अतिचालक इलेक्ट्रॉनिक्स के क्षेत्र में एक नई क्रांति ला दी है, क्योंकि इन्हें ऐसे तापमानों पर संचालित किया जा सकता है जो एकल-चरण क्रायोकूलर या तरल नाइट्रोजन द्वारा प्राप्त किए जा सकते हैं, जो तरल हीलियम या हीलियम-आधारित बहुस्तरीय क्रायोकूलर की तुलना में अधिक किफायती होता है। उच्च क्रांतिक तापमान (92 K) और बनाने की प्रक्रिया में आसानी के कारण,  $\text{YBa}_2\text{Cu}_3\text{O}_{7-x}$  (YBCO) सबसे उपयुक्त उच्च तापमान अतिचालक है। उच्च तापमान अतिचालकों पर आधारित जोसेफसन जंक्शन बनाने के कई तरीके हैं, जिनमें स्टेप एज जंक्शन को प्राथमिकता दी जाती है, क्योंकि इसे बनाना आसान होता है और इसे सबस्ट्रेट पर कहीं भी स्थापित किया जा सकता है। इससे जोसेफसन जंक्शनों का उच्च घनत्व वाला सरणी बनाना संभव हो जाता है। हालांकि, स्टेप एज जंक्शनों का  $I_c R_n$  गुणनफल (जिसे विशेष विभव वोल्टेज भी कहा जाता है) कम होता है और इसे बढ़ाने के लिए उपयुक्त तकनीकों की आवश्यकता होती है।

इस शोधकार्य में,  $\text{MgO}$  (100) सबस्ट्रेट पर स्टेप एज जोसेफसन जंक्शन का निर्माण किया गया है, जिसमें मानक फोटोलिथोग्राफी और आयन बीम नक्काशी तकनीकों का उपयोग किया गया है, जबकि अतिचालक फिल्म को स्पंदित लेजर निक्षेपण (PLD) तकनीक द्वारा बनाया गया है। स्टेप एज जोसेफसन जंक्शनों के गुणों को समायोजित करने के लिए स्टेप कोण और माइक्रोब्रिज की चौड़ाई के प्रभावों का अध्ययन किया गया है। स्टेप कोण को नियंत्रित करने के लिए आयन बीम के गिरने की दिशा को बदला गया, जिसे सबस्ट्रेट की विभिन्न दिशाओं में उन्मुख करके प्राप्त किया गया। स्टेप कोण को  $10^\circ$  से  $35^\circ$  तक बदला गया, जबकि माइक्रोब्रिज की चौड़ाई और लंबाई को क्रमशः  $10 \mu\text{m}$  और  $100 \mu\text{m}$  रखा गया। यह पाया गया कि स्टेप कोण बढ़ने के साथ, जंक्शन की क्रांतिक धारा ( $I_c$ ) घटती है जबकि इसका सामान्य अवस्था प्रतिरोध ( $R_n$ ) बढ़ता है। सभी तापमानों, (68 K से 77 K) पर  $I_c R_n$  गुणनफल में वृद्धि देखी गई।  $35^\circ$  स्टेप कोण वाले जंक्शन के लिए  $I_c R_n$  का मान 77 K पर 0.34 mV प्राप्त हुआ। कम स्टेप कोण वाले जंक्शनों में, अतिचालक से अतिचालक कण- युग्मन, अधिक अतिचालक- सामान्य-

अतिचालक (SNS) प्रकार का व्यवहार प्रदर्शित करता है, जबकि उच्च स्टेप कोण पर यह, अतिचालक-कुचालक-अतिचालक (SIS) व्यवहार प्रदर्शित करने लगता है। माइक्रोब्रिज की चौड़ाई का विद्युत परिवहन गुणों पर प्रभावों का अध्ययन करने के लिए, इसकी चौड़ाई को 20  $\mu\text{m}$  से 2  $\mu\text{m}$  तक बदला गया, जबकि स्टेप कोण  $\sim 19^\circ$  और माइक्रोब्रिज की लंबाई 100  $\mu\text{m}$  रखी गई। यह पाया गया कि माइक्रोब्रिज की चौड़ाई कम करने से क्रांतिक धारा ( $I_c$ ) घटती है और सामान्य अवस्था प्रतिरोध ( $R_n$ ) बढ़ता है, जबकि  $I_c R_n$  गुणनफल बढ़ता है। 2  $\mu\text{m}$  चौड़ाई वाले जंक्शन के लिए क्रांतिक धारा घनत्व का मान अधिकतम प्राप्त हुआ। सभी जंक्शन अतिचालक- सामान्य चालक- अतिचालक (SNS) प्रकार के पाए गए। 2  $\mu\text{m}$  माइक्रोब्रिज वाले जंक्शन के लिए  $I_c R_n$  गुणनफल 77 K पर 0.4 mV प्राप्त हुआ। जब स्टेप कोण  $\sim 35^\circ$  और माइक्रोब्रिज चौड़ाई 2  $\mu\text{m}$  ली गई, तो  $I_c R_n$  गुणनफल  $\sim 0.52$  mV प्राप्त हुआ। स्टेप एज जोसेफसन जंक्शन की सटीक प्रकृति को समझने के लिए, इसके I-V गुणों का प्रतिरोधी-धारिता संकुल जंक्शन (RCSJ) मॉडल का उपयोग करके अनुकरण किया गया और इसे  $35^\circ$  स्टेप कोण और, 2  $\mu\text{m}$  माइक्रोब्रिज चौड़ाई वाले जंक्शन के प्रयोगात्मक परिणामों से तुलना की गई। जब RCSJ मॉडल में केवल एक जंक्शन माना गया, तो अनुकरित डेटा प्रयोगात्मक डेटा से मेल नहीं खाया। लेकिन जब मॉडल में दो जोसेफसन जंक्शन श्रृंखला में जुड़े माने गए, तो अनुकरित डेटा और प्रयोगात्मक डेटा अच्छी तरह मेल खाए। विभिन्न तापमानों पर अनुकरित और प्रयोगात्मक I-V वक्रों की तुलना से पता चलता है, कि रव कारक, तापमान बढ़ने के साथ बढ़ता है।

जंक्शन के  $I_c R_n$  गुणनफल को और बढ़ाने के लिए एक अन्य संभावित विधि जंक्शन क्षेत्र में ऑक्सीजन रिक्तियों को बढ़ाना है, जो कि इस शोध में, 1 मिनट से 6 मिनट तक के विभिन्न समय अंतरालों के लिए जंक्शन क्षेत्र को आर्गन (Ar) आयनों के साथ विकिरणित करके प्राप्त किया गया है। 4 मिनट तक विकिरण के बाद, 77 K पर,  $I_c \sim 70 \mu\text{A}$  और  $R_n \sim 9.4 \Omega$  प्राप्त हुआ, जिससे  $I_c R_n$  गुणनफल  $\sim 0.66$  mV तक बढ़ गया।

अंततः, एक एकदिश धारा अतिचालक क्वांटम इंटरफेरेंस यंत्र (SQUID) को STO (100) सबस्ट्रेट पर स्टेप एज जोसेफसन जंक्शनों का उपयोग करके बनाया गया। इस SQUID में दो समानांतर स्टेप एज जोसेफसन जंक्शन हैं, जिनकी माइक्रोब्रिज चौड़ाई  $2 \mu\text{m}$ , लंबाई  $50 \mu\text{m}$  और लूप क्षेत्र  $20 \times 50 \mu\text{m}^2$  है। इसके विद्युत परिवहन गुणधर्मों, जैसे R-T, I-V, और वोल्टेज-फ्लक्स विशेषताओं का अध्ययन किया गया। इसके अलावा, कई तापीय चक्रों के साथ, यंत्र के क्रांतिक तापमान में गिरावट देखी गई और इसकी अस्थिरता में वृद्धि हुई। यंत्र की स्थिरता बढ़ाने के लिए, इसे S1813 प्रकाश- प्रतिरोध परत से निष्क्रिय किया गया। पाया गया कि निष्क्रियित यंत्र जल प्रतिरोधी बन गया, जिसका संपर्क कोण  $108^\circ$  था और यह नमी के लंबे समय तक संपर्क में रहने पर भी खराब नहीं हुआ। निष्क्रिय करने के बाद भी यंत्र के परिवहन गुणधर्मों में कोई बदलाव नहीं देखा गया, जिससे संकेत मिलता है कि YBCO आधारित यंत्रों को तरल नाइट्रोजन निम्नतापस्थायी में संचालित करने के लिए यह निष्क्रिय करने की तकनीक प्रभावी है। निष्क्रियित SQUID के वोल्टेज-फ्लक्स गुणधर्मों का अध्ययन  $6 \times 10^{-7}$  T चुंबकीय क्षेत्र पर किया गया। एक मॉड्यूलन अवधि  $1.2 \times 10^{-7}$  T चुंबकीय क्षेत्र के अनुरूप थी। इस SQUID की संवेदनशीलता  $\sim 10^{-10} \text{ THz}^{-1/2}$  प्राप्त हुई।

# TABLE OF CONTENTS

<b>CERTIFICATE.....</b>	<b>i</b>
<b>ACKNOWLEDGEMENTS.....</b>	<b>ii</b>
<b>ABSTRACT.....</b>	<b>v</b>
<b>TABLE OF CONTENTS.....</b>	<b>xi</b>
<b>LIST OF FIGURES .....</b>	<b>xvi</b>
<b>LIST OF TABLES .....</b>	<b>xx</b>
<b>LIST OF SYMBOLS .....</b>	<b>xxi</b>
<b>CHAPTER I: Introduction</b>	<b>1-30</b>
1.1 Overview.....	1
1.2 Basics of Superconductivity.....	4
1.2.1 Zero Resistivity.....	4
1.2.2 Perfect Diamagnetism.....	5
1.2.3 Types of Superconductors.....	6
1.2.4 Flux Quantization.....	7
1.3 High Temperature Superconductors.....	8
1.4 Yttrium Barium Copper Oxide (YBCO).....	8
1.4.1 Crystal Structure of YBCO.....	9
1.4.2 YBCO Synthesis Methods.....	10
1.4.3 YBCO Thin Films.....	11
1.5 Josephson Effect.....	13
1.6 Resistively Capacitively Shunted Junction Model.....	14
1.7 Superconducting Quantum Interference Device.....	16
1.8 Types of High Temperature Superconducting Josephson Junctions.....	18
1.9 Motivation of the Work.....	21

1.10 Objective of the Thesis.....	21
1.11 Outline of the Thesis.....	22
References.....	27
<b>CHAPTER II: Experimental Techniques</b>	<b>31-62</b>
2.1 Introduction.....	32
2.2 Synthesis and Palletization of YBCO.....	32
2.2.1 Preparation of YBCO Using Solid State Reaction Method.....	32
2.2.2 Preparation of YBCO Target for Film Deposition.....	34
2.3 Fabrication of Superconducting Devices.....	35
2.3.1 Pulsed Laser Deposition.....	35
2.3.2 Photolithography.....	38
2.3.3 Ion Beam Etching.....	41
2.4 Characterization Techniques.....	43
2.4.1 X- ray Diffraction.....	44
2.4.2 Field Emission Scanning Election Microscopy.....	46
2.4.3 Atomic Force Microscopy.....	50
2.4.5 Contact Angle Measurement.....	52
2.5 Closed Cycle Cryocooler.....	54
2.6 Electrical Transport Measurement Techniques.....	56
2.6.1 Resistance versus Temperature Measurement.....	56
2.6.2 Current-Voltage Measurement.....	57
2.6.3 Voltage-Flux Characteristics.....	58
References.....	61

**CHAPTER III: YBCO Step Edge Josephson Junctions With Varying Step  
Angles 63-79**

3.1 Introduction.....64  
3.2 Device Fabrication.....65  
    3.2.1 Fabrication of Step on MgO Substrate.....66  
    3.2.2 YBCO Film Deposition.....67  
    3.2.3 Fabrication of Microbridge Across the Step.....67  
3.3 Results and Discussion.....68  
    3.3.1 Atomic Force Microscopy Analysis.....68  
    3.3.2 X-ray Diffraction Analysis.....69  
    3.3.3 Resistance versus Temperature Measurement .....70  
    3.3.4 Current-Voltage Measurement.....71  
3.4 Conclusion.....77  
References.....78

**CHAPTER IV: YBCO Step Edge Josephson Junction With Varying  
Microbridge Widths 80-93**

4.1 Introduction.....81  
4.2 Device Fabrication.....81  
4.3 Results and Discussion.....82  
    4.3.1 Structural Analysis.....82  
    4.3.2 Surface Analysis.....83  
    4.3.3 Resistance versus Temperature Measurement.....84  
    4.3.4 Current-Voltage Measurement..... 85  
4.4 Conclusion.....91  
References.....92

**CHAPTER V: RCSJ Modeling of YBCO Step Edge Junction 94-107**

5.1 Introduction.....95

5.2 Device Fabrication.....96

5.3 Simulation Method.....96

5.4 Results and Discussion.....98

    5.4.1 Structural Analysis .....98

    5.4.2 Surface Analysis.....99

    5.4.4 Electrical Measurement.....100

    5.4.5 Simulation of the I-V curves of the Junction Using RCSJ model.....101

        5.4.5.1 Simulation Using RCSJ Model Considering Single Junction.....101

        5.4.5.2 Simulation Using RCSJ Model Considering Two Junctions.....101

        5.4.5.3. Simulation at Different Operating Temperatures.....102

5.5 Conclusion.....105

References.....106

**CHAPTER VI: Ar ion irradiation of YBCO Step Edge Junction 108-120**

6.1 Introduction.....109

6.2 Experimental Section.....110

    6.2.1 Device Fabrication.....110

    6.2.2 Ar Ion Irradiation of the Step Edge Junction.....110

6.3 Results and Discussion.....111

    6.3.1 Structural Analysis.....111

    6.3.2 Surface Analysis.....111

    6.3.3 Resistance versus Temperature Measurement.....112

    6.3.4 Current-Voltage Measurement.....113

6.4 Conclusion.....117

References.....119

**CHAPTER VII: YBCO Superconducting Quantum Interference Device and its  
Passivation 121-135**

7.1 Introduction.....122

7.2 Experimental Section.....123

    7.2.1 Device Fabrication.....123

    7.2.2 SQUID Characterizations.....124

7.3 Results and Discussion.....124

    7.3.1 Surface Analysis.....124

    7.3.2 Resistance versus Temperature Measurement.....126

    7.3.3 Current-Voltage Measurement.....126

    7.3.4 Contact Angle Measurement.....128

    7.3.5 Passivation of the Device.....128

    7.3.6 Current-Voltage Measurement of the Passivated Device.....131

    7.3.7 Voltage-Flux ( $V-\Phi$ ) characteristics of SQUID.....131

7.4 Conclusion.....133

References.....134

**CHAPTER VIII: Conclusion and Future Scope 136-141**

**List of Publications.....142**

**Author’s Biodata.....145**

## List of Figures

Figure No.	Figure Caption	Page No.
<b>Figure 1.1</b>	Variation of resistance with temperature for mercury.	<b>5</b>
<b>Figure 1.2</b>	Schematic showing the behaviour of a superconductor in an applied magnetic field.	<b>5</b>
<b>Figure 1.3</b>	Variation of magnetization with applied magnetic field for (a) type I and (b) type II superconductors.	<b>7</b>
<b>Figure 1.4</b>	Superconducting ring in the presence of an external magnetic field.	<b>7</b>
<b>Figure 1.5</b>	Crystal Structure of $\text{YBa}_2\text{Cu}_3\text{O}_7$ .	<b>10</b>
<b>Figure 1.6</b>	Schematic for the (a) Josephson junction and (b) DC Josephson effect.	<b>14</b>
<b>Figure 1.7</b>	Schematic diagram for the RCSJ model of a Josephson junction.	<b>15</b>
<b>Figure 1.8</b>	Schematic diagram for flow of screening current in SQUID for (a) $\Phi < \Phi_0/2$ , (b) $\Phi > \Phi_0/2$ , and (c) V- $\Phi$ characteristics of the SQUID.	<b>18</b>
<b>Figure 1.9</b>	Schematic showing the (a) natural grain boundary, (b) bicrystal grain boundary, (c) step edge grain boundary, and (d) Dayem bridge Josephson junction.	<b>20</b>
<b>Figure 2.1</b>	(a) Morter Pestle used for grinding (b) alumina boat (c) furnace used for calcination and sintering.	<b>33</b>
<b>Figure 2.2</b>	(a) Die (b) hydraulic press used for pelletizing the YBCO powder and (c) YBCO pellet obtained after the sintering process.	<b>34</b>
<b>Figure 2.3</b>	(a) Schematic diagram and (b) experimental setup of pulsed laser deposition system.	<b>37</b>
<b>Figure 2.4</b>	Experimental setup of the optical maskless lithography system.	<b>40</b>
<b>Figure 2.5</b>	Schematic diagram for Ion beam etching system.	<b>42</b>
<b>Figure 2.6</b>	Experimental setup of Ar Ion beam etching system for etching.	<b>43</b>
<b>Figure 2.7</b>	Schematic diagram of the diffraction phenomena of X-rays from the crystal planes.	<b>44</b>
<b>Figure 2.8</b>	Experimental setup of X-ray diffractometer.	<b>46</b>
<b>Figure 2.9</b>	Schematic showing (a) electron matter interaction and (b) various components of field emission scanning electron microscope.	<b>48</b>
<b>Figure 2.10</b>	Experimental setup of field emission scanning electron microscope	<b>50</b>
<b>Figure 2.11</b>	Schematic showing the (a) various components and (b) forces involved in the various operating modes of atomic force microscope.	<b>51</b>
<b>Figure 2.12</b>	Experimental setup of atomic force microscope.	<b>52</b>
<b>Figure 2.13</b>	Schematic showing the wettability of a material depending on its contact angle.	<b>53</b>
<b>Figure 2.14</b>	Experimental set up of contact angle measurement system.	<b>54</b>

<b>Figure 2.15</b>	Schematic showing various components of a closed cycle cryocooler.	<b>55</b>
<b>Figure 2.16</b>	Schematic showing the arrangement of contacts for R-T measurement of YBCO film.	<b>56</b>
<b>Figure 2.17</b>	(a) Schematic showing the arrangement of the contacts on the device for the I-V measurement. (b) Image of the device mounted on the cold head of cryocooler (c) Experimental setup for the electrical transport measurement.	<b>58</b>
<b>Figure 2.18</b>	Schematic showing the circuit used for voltage-flux measurement of SQUID.	<b>59</b>
<b>Figure 2.19</b>	Schematic showing the circuit used for voltage-flux measurement of SQUID in FLL mode.	<b>60</b>
<b>Figure 3.1</b>	Schematic diagram showing the process flow for fabricating a step edge Josephson junction.	<b>66</b>
<b>Figure 3.2</b>	Schematic of (a) ion beam falling on the photoresist-covered MgO substrate and (b) angle of incidence of the ion beam relative to the plane of the substrate.	<b>67</b>
<b>Figure 3.3</b>	(a) Schematic of the step edge where $\theta$ represents the step angle. AFM images of steps formed on MgO substrates with (b) $10^\circ$ , (c) $19^\circ$ , and (d) $35^\circ$ step angles.	<b>69</b>
<b>Figure 3.4</b>	XRD spectrum of YBCO thin film on MgO (100) substrate.	<b>70</b>
<b>Figure 3.5</b>	R-T measurement of YBCO (a) thin film and (b) step edge Josephson junction.	<b>71</b>
<b>Figure 3.6</b>	I-V characteristics of junctions with step angle (a) $10^\circ$ , (b) $19^\circ$ , and (c) $35^\circ$ and variation of $I_c$ , $R_n$ , and $I_cR_n$ values with temperature for step angle (d) $10^\circ$ , (e) $19^\circ$ , and (f) $35^\circ$ .	<b>72</b>
<b>Figure 3.7</b>	Variation of the values of (a) $I_c$ , (b) $R_n$ , (c) $I_cR_n$ for different step angles 77 K.	<b>74</b>
<b>Figure 3.8</b>	Variation of $J_c$ with reduced temperature ( $1-T/T_c$ ) for (a) $10^\circ$ , (b) $19^\circ$ , and (c) $35^\circ$ angled step edge Josephson junctions. Solid lines are the fitted curves.	<b>75</b>
<b>Figure 3.9</b>	Variation of $I_cR_n$ product with critical current density for samples with step angles $10^\circ$ , $19^\circ$ , and $35^\circ$ . Solid lines are the fitted curves.	<b>76</b>
<b>Figure 4.1</b>	Schematic of (a) 3D view (b) top view of step edge Josephson junction.	<b>82</b>
<b>Figure 4.2</b>	XRD spectrum of YBCO thin film on MgO (100) substrate.	<b>83</b>
<b>Figure 4.3</b>	(a) AFM micrograph of step edge on MgO substrate. FESEM images of the step edge Josephson junction with the width of the microbridge as (b) $20\ \mu\text{m}$ , (c) $10\ \mu\text{m}$ , (d) $5\ \mu\text{m}$ , and (e) $2\ \mu\text{m}$ .	<b>84</b>
<b>Figure 4.4</b>	R-T graphs of (a) YBCO film and (b) step edge junctions with varying widths of microbridge.	<b>85</b>

<b>Figure 4.5</b>	I-V curves of step edge junction for the junction with microbridge width as (a) 20 $\mu\text{m}$ , (b) 10 $\mu\text{m}$ , (c) 5 $\mu\text{m}$ , and (d) 2 $\mu\text{m}$ . $I_c$ , $R_n$ , and $I_cR_n$ product plotted with temperature for step edge Josephson junction having the width of microbridge (e) 20 $\mu\text{m}$ , (f) 10 $\mu\text{m}$ , (g) 5 $\mu\text{m}$ , and (h) 2 $\mu\text{m}$ .	<b>86</b>
<b>Figure 4.6</b>	(a) Variation of (a) $I_c$ , (b) $R_n$ , and (c) $I_cR_n$ product with the width of the microbridge at 77 K.	<b>88</b>
<b>Figure 4.7</b>	Variation of critical current density $J_c$ with the width of microbridge at 77 K.	<b>89</b>
<b>Figure 4.8</b>	Variation of $J_c$ with reduced temperature ( $1-T/T_c$ ) for step edge junctions with microbridge width of (a) 20 $\mu\text{m}$ , (b) 10 $\mu\text{m}$ , (c) 5 $\mu\text{m}$ , and (d) 2 $\mu\text{m}$ .	<b>90</b>
<b>Figure 4.9</b>	Variation of (a) $I_cR_n$ with $I_c$ and (b) $1/R_n$ for step edge junctions with varying widths of microbridge.	<b>91</b>
<b>Figure 5.1</b>	Schematic diagram representing the circuit considered in the RCSJ model.	<b>97</b>
<b>Figure 5.2</b>	XRD spectrum of YBCO thin film on MgO (100) substrate.	<b>100</b>
<b>Figure 5.3</b>	(a) AFM micrograph of step on the substrate, (b) SEM micrograph of the device, and (c) magnified image of the junction area.	<b>99</b>
<b>Figure 5.4</b>	(a) R-T graph and (b) I-V curve (at 77 K) of step edge junction.	<b>100</b>
<b>Figure 5.5</b>	Experimental I-V curve of the step edge junction and its fitting using single junction RCSJ model for step edge junction.	<b>101</b>
<b>Figure 5.6</b>	Fitting of I-V data using double junction RCSJ model for step edge junction.	<b>102</b>
<b>Figure 5.7</b>	I-V characteristics of step edge junction at (a) 68 K (b) 72 K (c) 80 K. Black lines are the experimental curves, and red lines are the I-V curves simulated using the RCSJ model.	<b>103</b>
<b>Figure 5.8</b>	Variation of $J_c$ of step edge junction with reduced temperature ( $1-T/T_c$ ).	<b>105</b>
<b>Figure 6.1</b>	Schematic showing process of Ar ion irradiation of junction area.	<b>110</b>
<b>Figure 6.2</b>	XRD spectrum of YBCO thin film on MgO (100) substrate.	<b>111</b>
<b>Figure 6.3</b>	(a) AFM image of the step etched MgO substrate (b) SEM image of the step edge junction.	<b>112</b>
<b>Figure 6.4</b>	R-T curve for (a) the YBCO thin film and (b) step edge Josephson junctions with different ion exposure time intervals and (c) variation of critical temperature ( $T_c$ ) of junctions as a function of irradiation time (t).	<b>113</b>
<b>Figure 6.5</b>	I-V characteristics of step edge junction irradiated for (a) 0 min (JJ0), (b) 1 min (JJ1), (c) 2 min (JJ2), and (d) 4 min (JJ4). $I_c$ , $R_n$ , and $I_cR_n$ products plotted as a function of temperature for (e) JJ0, (f) JJ1, (g) JJ2, and (h) JJ4.	<b>114</b>
<b>Figure 6.6</b>	Variation of (a) $I_c$ , (b) $R_n$ , and (c) $I_cR_n$ product with Ar ion irradiation time (t) at 77 K.	<b>116</b>

<b>Figure 6.7</b>	Variation of $J_c$ with reduced temperature ( $1-T/T_c$ ) for JJ0, JJ1, JJ2, and JJ4.	<b>117</b>
<b>Figure 7.1</b>	Schematic showing the process flow involved in the fabrication of step edge Josephson junction based SQUID.	<b>125</b>
<b>Figure 7.2</b>	Schematic of step edge Josephson junction-based SQUID.	<b>125</b>
<b>Figure 7.3</b>	(a) Height profile of the step taken using AFM and (b) SEM image of the SQUID.	<b>127</b>
<b>Figure 7.4</b>	Variation of resistance with temperature for SQUID.	<b>126</b>
<b>Figure 7.5</b>	I-V characteristics of the SQUID at 77 K.	<b>127</b>
<b>Figure 7.6</b>	Variation of critical temperature of the bare SQUID with number of thermal cycles.	<b>127</b>
<b>Figure 7.7</b>	Contact angle measurement bare SQUID in continuous contact with water droplet for (a) 0 min, (b) 5 min, (c) 10 min, and (d) 15 min.	<b>128</b>
<b>Figure 7.8</b>	(a) Contact angle measurement of passivated SQUID in continuous contact with a water droplet for 30 min. (b) Image showing the passivated device after spraying water onto it.	<b>129</b>
<b>Figure 7.9</b>	R-T measurement of the bare and the passivated SQUID.	<b>130</b>
<b>Figure 7.10</b>	Variation of critical temperature of the passivated SQUID with number of thermal cycles.	<b>130</b>
<b>Figure 7.11</b>	I-V characteristics of the SQUID at 77 K.	<b>131</b>
<b>Figure 7.12</b>	Schematic showing circuit used for measuring the voltage-flux characteristics of the SQUID.	<b>132</b>
<b>Figure 7.13</b>	V- $\Phi$ characteristics of the SQUID.	<b>132</b>

## List of Tables

<b>Table No.</b>	<b>Table Caption</b>
<b>Table 1.1</b>	Various single crystal substrates used for YBCO thin film deposition.
<b>Table 5.1</b>	Values of different parameters used for the simulation of I-V curves.

## List of Symbols

---

<b>Symbol</b>	<b>Description</b>
<b>H</b>	Applied Magnetic Field
<b>I<sub>bias</sub></b>	Bias Current
<b>k<sub>B</sub></b>	Boltzmann's constant
<b>C</b>	Capacitance
<b>ξ</b>	Coherence Length
<b>H<sub>c</sub></b>	Critical Magnetic Field
<b>T<sub>c</sub></b>	Critical Temperature
<b>I</b>	Current
<b>e</b>	Electronic Charge
<b>f</b>	Frequency
<b>λ<sub>j</sub></b>	Josephson Penetration Depth
<b>H<sub>c1</sub></b>	Lower Critical Magnetic Field
<b>λ<sub>L</sub></b>	London Penetration Depth
<b>Φ</b>	Magnetic Flux
<b>Φ<sub>0</sub></b>	Magnetic Flux Quantum
<b>M</b>	Magnetization
<b>R<sub>n</sub></b>	Normal State Resistance
<b>h</b>	Plank's Constant
<b>λ</b>	Penetration Depth
<b>μ<sub>0</sub></b>	Permeability of Free Space
<b>ħ</b>	Reduced Plank's Constant
<b>R</b>	Resistance

<b><math>\beta_c</math></b>	Stewart-McCumber Parameter
<b><math>\Delta</math></b>	Superconducting Energy Gap
<b><math>\delta</math></b>	Superconducting Phase
<b><math>I_s</math></b>	Supercurrent
<b>T</b>	Temperature
<b>D</b>	Thermal Noise Intensity
<b><math>H_{c2}</math></b>	Upper Critical Magnetic Field
<b>V</b>	Voltage
<b>w</b>	Width of Microbridge